Atmos. Chem. Phys. Discuss., 7, 11091–11121, 2007
www.atmos-chem-phys-discuss.net/7/11091/2007/

Atmospheric Chemistry and Physics Discussions

Observations of the effects of temperature on atmospheric HNO_3, ΣANs, ΣPNs, and NO_x: evidence for a temperature dependent HO_x source

D. A. Day[1], **P. J. Wooldridge**[1], **and R. C. Cohen**[1,2,3]

[1]Department of Chemistry, UC Berkeley, USA
[2]Department of Earth and Planetary Science, UC Berkeley, USA
[3]Energy and Environment Technologies Division, Lawrence Berkeley National Laboratory, USA

Received: 5 July 2007 – Accepted: 18 July 2007 – Published: 26 July 2007

Correspondence to: R. C. Cohen (rccohen@berkeley.edu)

Abstract

We describe observations of atmospheric reactive nitrogen compounds including NO, NO_2, total peroxy nitrates, total alkyl nitrates, and HNO_3 and their correlation with temperature. The measurements were made at a rural location 1315 m a.s.l. on the western slope of the Sierra Nevada Mountains in California during summer of 2001. The ratio of HNO_3 to its source molecule, NO_2, and the ratio of HNO_3 to all other higher oxides of nitrogen (NO_z) all increase with increasing temperature. Analysis of these increases suggests they are due to a steep increase in OH of between a factor of 2 and 3 over the range 18–32°C. Total peroxy nitrates decrease and total alkyl nitrates increase over the same temperature range. The decrease in the total peroxy nitrates is shown to be much less than expected if the rate of thermal decomposition were the sole important factor and to be consistent with the increase in OH inferred from the temperature trends in the HNO_3/NO_2 ratio.

1 Introduction

Observations and models show surface concentrations of ozone generally increase with temperature (e.g., Cardelino and Chameides, 1990; Olszyna et al., 1997; 1995). Since predictions are that global temperatures and regional heatwaves will occur with increasing frequency as greenhouse gases accumulate in the atmosphere, understanding the mechanisms responsible for the temperature dependence of O_3 is receiving renewed attention (e.g., Hogrefe et al., 2004; Leung and Gustafson, 2005; Murazaki and Hess, 2006; Steiner et al., 2006; Stevenson et al., 2005). High temperatures are known to be correlated with stagnation events which are one factor responsible for the ozone temperature correlations. Observations and models also show that the anthropogenic (Rubin et al., 2006; Stump et al., 1992; Welstand et al., 2003) and biogenic (Lamb et al., 1987; Wiedinmyer et al., 2005) VOC emissions that are precursors to ozone increase with temperature, a second factor responsible for the

ACPD

7, 11091–11121, 2007

temperature ozone correlations. However, the temperature response of NO_x, the other major precursor to ozone and of more oxidized nitrogen oxides (peroxy nitrates, alkyl and multifunctional nitrates and HNO_3) which are co-products of ozone production, is much less well established.

In a comprehensive modeling study, Sillman and Sampson (1995) described calculations of NO_y partitioning as a function of temperature for several locations. They discussed the role of the steep temperature dependence of the thermal decomposition rate for PAN on the response of ozone to temperature concluding, that "PAN chemistry appears to have an equal or greater impact than the more obvious causes of the temperatures dependence, i.e., insolation, H_2O, or increased emission of isoprene." The only corresponding experimental study of the relationship of temperature to nitrogen oxides is the study by Olszyna et al. (1997) who describe summertime observations of PAN/NO_y for a range of temperature and the contribution of NO_x, PAN, HNO_3, particulate nitrate, and total NO_z to NO_y for two different temperatures at a rural site. They observe that, as a fraction of NO_y, PAN and NO_x decrease with temperature, HNO_3 and particulate nitrate change very little, while NO_z and an unidentified contribution to NO_y (that they attribute as likely due to alkyl nitrates) increase with temperature. They suggest that the shift from PAN to the unidentified NO_z component at higher temperatures may be the result of the change in the PAN thermal equilibrium providing increased NO_x and RO_2 for alkyl and multifunctional nitrate production.

In this manuscript, we describe observations of atmospheric reactive nitrogen compounds including NO, NO_2, total peroxy nitrates (ΣPNs), total alkyl nitrates (ΣANs), and HNO_3 and their correlation with temperature. The measurements were made at a rural location 1315 m a.s.l. on the western slope of the Sierra Nevada Mountains in California during summer of 2001. The site has an extremely regular meteorology and the regional transport pattern is not strongly correlated with temperature during the summer (Dillon et al., 2002; Murphy et al., 2006a; Murphy et al., 2006b, and references therein). The transport pattern results in arrival of a plume originating in the city of Sacramento, CA, 50 km upwind at the University of California-Blodgett Forest Re-

ACPD
7, 11091–11121, 2007

search Station almost every day with little variation in transit time. As a consequence of this regularity, all of the observations we present are from a single source region and observations within a single season provide sufficient statistics to examine the correlations between temperature and the abundance of the various nitrogen oxides.

2 Measurements and site description

Measurements described in this paper were made from June–September, 2001 near the University of California – Blodgett Forest Research Station (UC-BFRS) (1315 m a.s.l., 38.9° N, 120.6° W). The site is a managed ponderosa pine plantation located in the mid Sierra Nevada Mountains 75 km northeast of Sacramento, CA (pop. 410 000, Greater Sacramento Area ≅ 2 million) in a sparsely populated region. The climate at this site is discussed in detail in Dillon et al. (2002) and Kurpius et al. (2002). Briefly, the climate of the western Sierras has a wet and a dry season. The dry season (May through September) is characterized by warmer temperatures, low rainfall, clear skies, and steady, regular east/west, upslope/downslope winds. The wet season (October-April) is characterized by cooler temperatures, moderate rainfall or snowfall, and less regular wind patterns. Temperatures peak in summer (June-August) and are lowest in late-fall through winter. During the dry season, upslope winds of 2–3 m/s from the southwest prevail during the day, switching at the hours of 18–19 (local time) to downslope winds of 0.5–2 m/s from the northeast with a return to southwesterlies at 7–8 in the morning. Very few days during the dry season are an exception to this pattern. Summer measurements described in this paper were characterized by almost no precipitation (<3 cm total), consistently warm temperatures (average daily peak ($\pm 1\sigma$)=24.4±3.7°C). Temperatures warmed by 3–5 degrees °C from early June reaching a peak in August. During summer, synoptic timescale temperature shifts occur on timescales of 2–7 days and can have magnitudes of as much as 10°C temperature swings (Fig. 1). Even in the presence of these synoptic variations, the mountain/valley wind pattern persists and results in the air at the site arriving from the west

bringing with it the urban plume from Sacramento, CA and it suburbs on more than 9 out of 10 days.

The role of transport and anthropogenic emissions in the summertime Sacramento plume as observed at the UC-BFRS are described by Dillon et al. (2002) and Murphy et al. (2006a, b, c). Briefly, the upslope/downslope flow pattern that characterizes transport in the western Sierras imposes a regular pattern on concentrations of chemicals that have their source in the Greater Sacramento Area. The concentrations of these compounds increase throughout the day during the upslope flow from the southwest (245 degrees). Downslope flow from the northeast (50 degrees) returns cleaner air to the site with minimum concentrations observed in the early to mid morning. Concentrations of long-lived species (e.g. acetylene) typically begin to increase at noon and reach their peak at 22 h, 2–3 h after the shift to downslope flow suggesting the center of the plume is slightly to the north of the UC-BFRS. Concentrations drop gradually after the 22 h peak reaching a minimum in mid-morning (10:00 a.m. local time). The concentrations of reactive species also exhibit strong variations with day-of-the-week due to variations in urban NO_x emissions and the resulting day-of-the-week patterns in OH concentrations (Murphy et al., 2006b, c).

A 10 m walk-up tower was used as a sampling platform in order to sample air above the tree canopy. Gas inlets and supporting equipment were mounted on the tower and accompanying analytical instrumentation was housed in a small wooden shed and a modified refrigerated shipping container with temperature control at the base of the tower.

Thermal dissociation – laser induced fluorescence (TD-LIF) was used to measure NO_2, total peroxy nitrates (ΣPNs), total alkyl nitrates (ΣANs), and HNO_3 at the UC-BFRS. The TD-LIF technique is described in detail in Day et al. (2002), application of the technique is described in Day et al. (2003), Murphy et al. (2006a), Rosen et al. (2004), and Cleary et al. (2007) and comprehensive details of the instrument, inlet, calibration and maintenance protocols for the measurements used in this analysis are described in Day (2003). Briefly, LIF detection of NO_2 comprises the core detection of

TD-LIF (Thornton et al., 2000). For the UC-BFRS TD-LIF instrument as set up from 2001–2005, an ambient sample flows rapidly through an inlet and is immediately split into four channels. The first one is used to observe NO_2; the second is heated to 180°C causing thermal dissociation (TD) of ΣPNs, the third to 350°C for additional TD of ΣANs, and the fourth to 550°C to include TD of HNO_3. The dissociation of all of these species produces NO_2 with unit efficiency. The NO_2signal in each channel is the sum of the NO_2 contained in all of the compounds that dissociate at the inlet temperature or below. Differences between the NO_2 signals observed simultaneously from channels heated to adjacent set-points are used to derive absolute abundances of each of these four classes of NO_y. The technique has the advantage that it measures the total contribution to NO_y in each class. For example, ΣPNs are expected to be predominantly PAN (peroxyacetyl nitrate), PPN (peroxypropionyl nitrate), and MPAN (peroxymethacryloyl nitrate). The measurement includes these three and all other peroxy and acyl peroxy nitrates and N_2O_5. However, we do not expect non-acyl peroxy nitrates or N_2O_5 to be present in significant concentrations in the summer, daytime boundary layer that is the focus of in this paper. Laboratory experiments show that the HNO_3 channel measures the sum of gas phase HNO_3 and thermally labile HNO_3 aerosols such as NH_4NO_3 with near unit efficiency. Confirmation of this laboratory result with field data is available from comparisons of TD-LIF measurements and PILS aerosol nitrate measurements under conditions where NH_3 was sufficiently high that nearly 100% of the HNO_3 was aerosol NO_3^- (Fountoukis et al., 2007). Salts such as $NaNO_3$ are not detected (Bertram and Cohen, 2003). Similarly, ΣANs are calculated to consist of all alkyl and multifunctional nitrates present in the gas or aerosol phase. Inorganic nitrate aerosols were reported to contribute 25% to measured inorganic nitrate (HNO_{3gas} + $NO^-_{3\ particulate}$) in the mid-Sierras during summer (Zhang et al., 2002). Measurements of NH_3 at the UC-BFRS during summer 2006 (Fischer and Littlejohn, submitted 2007) show that concentrations are too low and temperatures too high to support NH_4NO_3 aerosol providing an indication that any aerosol NO_3^- in the region is non-volatile and would not have been detected as part of our measurements of HNO_3. Comparison of ΣNO_{yi}

($\Sigma NO_{yi} \equiv$ NO (measured by chemiluminescence) + NO_2 + ΣPNs + ΣANs + HNO_3) and total NO_y (measured by catalysis – chemiluminescence) shows that these two values are usually within 10% of each other (Day et al., 2003; Dillon, 2002). Measurements of NO were made at the UC-BFRS using NO-O_3 chemiluminescence (Thermo Environmental Co. model 42CTL). Wind speed, wind direction, humidity, temperature, CO_2 and O_3 concentrations, net radiation, photosynthetically-active radiation, and pressure were measured as described in Goldstein et al. (2000) and Bauer et al. (2000).

3 Results and analysis

During the summer, anthropogenic emissions in the region of the study are dominated by those from motor vehicles and have a strong weekday vs. weekend variation. To eliminate this variable from our analysis, we present data from Tuesday through Friday. Observations on Saturday through Monday are consistent with our conclusions but have lower overall NO_y because of reduced weekend emissions in Sacramento and because of the approximately two-day memory for emissions within the region (Murphy et al., 2006b, c). Figure 1 shows the afternoon (12–16 h) medians of O_3 and the reactive nitrogen species for each day of the summer 2001. Figure 2 shows the diurnal cycles of O_3, ΣNO_{yi}, NO_x, ΣPNs, ΣANs, and HNO_3 with half-hour time resolution. We represent the effects of temperature throughout each day by a single variable, the maximum daily temperature observed at UC-BFRS during the afternoon. We define a day as starting at 05:00 a.m. just prior to change of direction in the airflow from downslope to upslope. The daily upslope/downslope behavior observed at this site is apparent in the diurnal cycles of ΣNO_{yi}, NO_x, ΣPNs, and O_3. HNO_3 is much more strongly affected by local photochemistry than any of these species and its diurnal cycle more closely tracks the solar zenith angle than it does the transport patterns. This effect has been observed at many other surface sites (e.g. Brown et al., 2004; Kleinman et al., 1994; Lefer et al., 1999; Parrish et al., 1986). The pattern in the ΣANs is weak, but is closer to one that is transport dominated than one that is controlled by

local photochemistry.

The clearest signatures of the effects of temperature can be seen in the mixing ratios of ozone, ΣANs and HNO_3 all of which have higher mixing ratios at high temperatures. The blue (colder) and red (warmer) lines in Fig. 2 represent the 17^{th} and 83rd percentile of the measurements as ordered by the associated T_{max}. Figure 3 shows the median afternoon (12–16 h) $NO_x/\Sigma NO_{yi}$, $\Sigma PNs/NO_z$, $\Sigma ANs/NO_z$, and HNO_3/NO_z ratios vs. T_{max}, where $NO_z \equiv \Sigma PNs + \Sigma ANs + HNO_3$. Lines representing a least-squares fit to the data are shown. The correlations of $\Sigma PNs/NO_z$(slope = -0.023 ppb/°C, R^2= 0.52) and HNO_3/NO_z (slope = 0.019 ppb/°C, R^2= 0.37) with temperature are strong with opposite signs. Both $NO_x/\Sigma NO_{yi}$ (slope=–0.0048 ppb/°C, R^2=0.14) and $\Sigma ANs/NO_z$ (slope=0.0036 ppb/°C, R^2=0.069) exhibit weaker correlations with temperature. Despite the low R^2 values, one can see that the lines shown do capture the major patterns present in the data. Figure 4 shows absolute concentrations of NO_x, ΣNO_{yi}, NO_z, and O_3 vs. temperature. NO_x concentrations show no significant increase or correlation, ΣNO_{yi} and NO_z exhibit weak positive correlations and increases of approximately 25%, and O_3 shows a strong positive correlation with an increase of more than 30 ppbv.

The timing of the diurnal cycles of the individual species or classes of reactive nitrogen (Fig. 2) are similar for the two temperature ranges indicating that contributions of the major processes affecting their mixing ratios remain similar, independent of temperature. The most notable effects of temperature on the concentrations are the large increases in the HNO_3, ΣANs and O_3 with increasing temperature. In contrast, as a fraction of NO_z, the decreases in ΣPNs and the increases in HNO_3 stand out more strongly than the change in the fraction of NO_z represented by ΣANs. Despite the near doubling of ΣANs mixing ratios for much of the day (Fig. 2) the ratio of ΣANs to NO_z during afternoon increases by only ~30% with a weak correlation with temperature. NO_x/NO_y, which is often used as a surrogate for photochemical processing or age of air (e.g. Olszyna et al., 1994; Williams et al., 1997) also exhibits a weak negative correlation with temperature. The complementary function NO_z/NO_y has a correlation

ACPD
7, 11091–11121, 2007

coefficient of R^2=0.14 and slope of 0.0048°C^{-1}. This correlation and slope are much smaller than reported by Olszyna et al. (1997) who describe the NO_z/NO_y correlation with temperature and indicate it has a correlation coefficient of R^2=0.81 and slope 0.042°C^{-1}. However, at higher temperatures, where Olszyna et al. (1997) observe a larger degree of processing of the plume (NO_z/NO_y >0.7) the correlation and magnitude of slope diminishes dramatically. All but one of the observations shown in Fig. 3 have NO_z/NO_y >0.7, thus a direct comparison of the two data sets can be misleading as the range in NO_x/NO_y does not overlap.

3.1 Transport

Observations of local wind speeds and duration do not support any correlation between warmer temperatures and increased flow from the Sacramento Valley. Winds are very consistent during the summer. There was a slight, but weak anti-correlation between wind speeds and temperature which would be expected to slow the arrival of the anthropogenic plume from Sacramento and result in lower CO, NO_y and other chemicals which are predominantly emitted in Sacramento and then transported to the site. Nevertheless, we observe a weak correlation of CO with temperature (R^2=0.10) that corresponds to a 35% increase from 18–32°C. In addition, VOC's measured at the UC-BFRS for 2 months during summer 2001 (with lifetime >4.5 h for OH = 1×10^7: butane, i-butane, hexane, methanol, propyne, toluene, pentane, and acetone) all had correlation coefficients of 0.10 or less with some increasing and others decreasing with temperature. While the evidence is at best equivocal, it can support no more than a 35% increase in the concentration of CO and VOC species carried by the urban plume. Based on the observed slope of the CO vs. ΣNO_{yi} correlation this can amount to no more than 20% increase in NO_2. It is likely that much of the CO increase is biogenic and that therefore the NO_x increase is much smaller than even this upper limit.

3.2 HNO_3

Each of the different classes of NO_y provides some insight into the mechanisms that are responding to changes in temperature. The relationship of HNO_3 mixing ratios with temperature for the data set is approximately linear increasing from 0.46 ppb at 18°C to 1.4 ppb at 32°C with a slope 0.067 ppb/°C and an R^2=0.50. During the daytime, the concentration of the HNO_3 can be approximately described as a stationary state between chemical production and losses to deposition and dilution:

$$k_{OH+NO_2}[OH][NO_2] = \frac{V_{dep}}{H_{ml}}[HNO_3] + K_{dil}\left([HNO_3] - [HNO_3]_{bg}\right) \quad (1)$$

where V_{dep} is the deposition velocity (0.034 m/s, Farmer and Cohen, 2007), H_{ml} is the mixed layer height (~800 m, Carroll and Dixon, 1998; Dillon et al., 2002; Seaman et al., 1995), K_{dil} is the dilution rate constant including both vertical venting and horizontal diffusion of the plume into the background air (~0.23 h^{-1}, Dillon et al., 2002), and $[HNO_3]_{bg}$ is the background nitric acid concentration into which the plume is diluted. We estimate that the free-tropospheric $[HNO_3]_{bg}$ for this region is roughly 200 ppt which is the intercept of the plot of $[HNO_3]$ vs. $[H_2O]$ for observations discussed in Murphy et al. (2006a) at a site at higher elevation in the Sierras which was often effected by free tropospheric air. Rearranging,

$$\frac{[HNO_3]}{[NO_2]} = \frac{k_{OH+NO_2}[OH] + K_{dil}[HNO_3]_{bg}/[NO_2]}{\frac{V_{dep}}{H_{ML}} + K_{dil}} \quad (2)$$

For NO_2=0.6 ppb, OH=1×10^7 molecules/cm^3 and k_{OH+NO2}=9.90×10^{-12} cm^3 molecules^{-1} s^{-1} (Sander et al., 2006), the lifetime of 1 ppb of HNO_3 with respect to production is approximately 5 h, the lifetime of HNO_3 with respect to deposition ($\tau_{dep}=H_{ml}/V_{dep}$) during the day is about 6.5 h, and the lifetime of HNO_3 due to the combination of deposition and dilution is about 2.6 h. HNO_3 is produced more rapidly

upwind where the $NO_2$and probably the OH concentrations are higher (Murphy et al., 2006c) and thus, at the UC-BFRS, HNO_3 concentrations are likely slightly higher than would be achieved in steady-state because the transport source of HNO_3 is significant. Nonetheless, the steady-state expression above provides a reasonable approximation for thinking about HNO_3. Similar equations relating HNO_3, NO_2, and OH,, without the dilution term, have been presented previously (Brown et al., 2004; Parrish et al., 1986).

NO_2 concentrations, the rate constant for the OH+NO_2 reaction, the boundary layer height, the deposition velocity and the dilution rate do not vary strongly with temperature. Thus, the only variable in Eqs. (1) and (2) that can explain the increase in HNO_3 with temperature is OH. We calculate afternoon OH concentrations using the relationship shown in Eqs. (1) and (2) (and the values for other parameters discussed above). We estimate the average temperature within the 800 m mixed layer (T_{ml}) using surface temperatures and the environmental lapse rate (6.5°C/km), resulting in temperatures approximately 3 °C lower than surface temperatures. A linear fit to the correlation plot of OH vs. T_{ml} yields an increase in OH from 8 x 10^6 molecules/cm^3 at T_{ml}=15°C to 2.4×10^7 molecules/cm^3 at T_{ml}=29×C, a 3-fold increase. Figure 5 shows the median afternoon (12–16 h) HNO_3/NO_2 data vs. T_{ml} (red circles). Also shown are modeled values for the HNO_3/NO_2 ratio calculated using the linear best fit line of the OH vs. T_{ml} correlation plot and Eq. (2). The coincident best fit lines are also shown. The scatter in the modeled data is due solely to the HNO_3 and NO_2 data since the other variables are either constant or vary linearly with temperature. The linear fit captures the general trend in the HNO_3/NO_2 data suggesting that a linear relationship between OH and T is reasonable.

The more rapid conversion of NO_2 to HNO_3 implied by this higher OH must also be accompanied by additional temperature dependent sources of NO_2 since the NO_2 remains nearly constant. The total of all NO_{yi} species that we observe, ΣNO_{yi}, also increases with temperature by about 25%, a fact that is somewhat surprising since increases in HNO_3 should be associated with more rapid deposition and removal of

ACPD
7, 11091–11121, 2007

NO_y. Likely temperature dependent sources of NO_2 include the thermal decomposition of PNs, a decrease in the dilution rate, and an increase in soil NO_x emissions. These factors are discussed further in the sections below.

As discussed above, we expect that the OH concentrations predicted using the steady state calculation and concentrations at the UC-BFRS is an overestimate of the OH responsible for producing the observed HNO_3 since NO_2 conditions are elevated upwind. Without a more detailed model, estimating the effective NO_2 for use in Eqs. (1) and (2) is difficult. To bracket the amount of $NO_2$and thus the absolute value of OH we compare an estimate using a 3 times larger value of NO_2 and calculate OH of 2.7×10^6 and 8×10^6 molecules/cm^3 for the two temperature extremes. This is a factor of three lower OH but the trend with temperature is still large, an increase of about a factor of 3. Both calculations produce OH estimates in the range of the average OH concentration ($1.1\pm0.5\times10^7$ molecules/cm^3) in the Sacramento plume for the 5-hour transect from Folsom, CA to the UC-BFRS that Dillon et al. (2002) calculated using a Lagrangian model and VOC measurements. That model represented a single average daily maximium temperature of 25°C.

3.3 ΣPNs

ΣPNs are approximately in thermal equilibrium with peroxyacyl radicals and NO_2 under warm boundary layer conditions (Cleary et al., 2007):

$$K_{PN_i}(T)=\frac{[PN_i]}{[PA_i][NO_2]} \quad (3)$$

Where $K_{PNi}(T)$ is the equilibrium constant, for each respective PN. This equilibrium is established through the reactions:

$$PA_i + NO_2 \rightarrow PN_i \quad (R1)$$

$$PN_i \rightarrow PA_i + NO_2 \quad (R2)$$

which determine the partitioning of the PN reservoir between the stable PN_i and its radical partner PA_i. In, addition, peroxyacyl radicals are also approximately in photochemical steady state with their sources and sinks (Cleary et al., 2007). Consider the case for the most common peroxyacyl nitrate, peroxyacetyl nitrate (PAN) and the peroxyacetyl radical (PA). The primary reactions that contribute to net formation and loss of the sum of PA and PAN include:

$$\text{acetaldehydeormethyglyoxal} + OH(+O_2) \rightarrow PA + H_2O \quad \text{(R3)}$$

$$PA + NO \rightarrow \text{Products} \quad \text{(R4)}$$

$$PA + HO_2 \rightarrow \text{Products} \quad \text{(R5)}$$

$$PA + RO_2 \rightarrow \text{Products}. \quad \text{(R6)}$$

Solving for the steady-state concentration of PA+PAN we derive:

$$[PA + PAN]_{ss} = \frac{k_3\,[\text{acetaldehyde(methyglyoxal)}]\,[OH]}{k_4[NO] + k_5[HO_2] + k_6[RO_2]}(1 + K_{PAN}[NO_2]) \quad (4)$$

We estimate the average temperature within the boundary layer using surface temperatures and the environmental lapse rate as discussed above in the HNO_3 section. From 15 to 29°C the equilibrium constant controlling the ratio of PA_i to PN_i decreases by a factor of 9 for PAN and PPN (Sander et al., 2006) respectively. Using the observed ΣPN and NO_2 concentrations and the equilibrium constant for PAN, we calculate the sum of all peroxyacyl radicals during mid-afternoon in the boundary layer finding a 5-6-fold increase from ~0.7 ppt to 3.7 ppt for the 15–29°C range of boundary layer average temperature. Trainer et al. (1991) examined observations at Scotia, PA in the summertime and calculated an increase in peroxyacyl radicals from 8–14 ppt over the temperature range from 26–32°C.

Since all of the losses of PA+PN are through the reactions of the radical, if all other factors were constant, this increase in PA radical concentrations implies a roughly 5–6

fold increase in the loss rate of ΣPNs during transport to UC-BFRS. The decrease we observe is much smaller, only about 30%, a fact that implies a nearly 5–6 fold increase in the source of ΣPNs. Two factors are primarily responsible:

1. A doubling of acetaldehyde and an implied increase in methylglyoxal associated with isoprene emissions and oxidation and a 10-fold increase of methacrolein with temperature. Both of these represent increases sources of two of the major peroxyacyl radicals.

2. A large increase in OH.

If we assume a 3-fold increase in OH and a 2-fold increase in ΣPN source aldehydes then the product is equal to the 6-fold increase in sources that we calculate and is consistent with the increase in OH estimate from the HNO_3/NO_2 ratio.

The net ΣPN decrease with T that we observe at Blodgett Forest corresponds to a release of about 500 ppt of NO_2 at the site. However, at UC-BFRS we observe a negligible change in NO_x with temperature implying almost all of this 500 ppt has gone to increases in the HNO_3 (and ΣAN) production during the transit of the plume to UC-BFRS. If we assume that this increased NO_x was present upwind of Blodgett Forest, where most of the HNO_3 we observe at UC-BFRS is produced, then the increase in OH needed to reproduce the changes in HNO_3/NO_2 is calculated to be smaller than the ~3-fold increase calculated using constant NO_2. Since PNs are only about 20% of NO_2 at Granite Bay (Murphy et al., 2006a), the effective increase in NO_2 with T integrated over the transect is likely no more than 20% and the OH required to produce HNO_3 is then calculated to be only 20% smaller than when we neglect this effect.

3.4 ΣANs

ΣANs increase by 250 ppt, 75% with temperature (Fig. 2) and by +45% and +30% as a fraction of NO_y and NO_z (Fig. 3), respectively. Quantitative interpretation of these increases is difficult because VOC precursors and their oxidation rates due to OH are

increasing. In addition, the lifetime of ΣANs with respect to OH and O_3 is highly uncertain because it is not known what fraction of reactions of OH with ΣANs produce multifunctional ΣAN products and what fraction produce NO_2 or HNO_3. (See Farmer and Cohen (2007) for additional discussion of this issue). Inspection of the diurnal cycle of ΣANs in Fig. 2 suggests that ΣAN increases may be, in part, due to nighttime chemical production. Evaluation of the effects of temperature on nighttime chemistry are interesting, but beyond the scope of this manuscript.

3.5 NO_x and NO_y

In addition to the effects of ΣPNs discussed above, an increase in the source of NO_x with temperature may be explained by increased NO_x soil emissions. Herman et al. reported that NO_x soil emissions in an oak forest in the Sierra Nevada foothills had fluxes of 5.8–15 ppt m s^{-1} (under canopy/open area with mean soil temperatures of ~24/28°C) (2003). Farmer and Cohen use an observationally constrained model to calculate a NO_x flux from UC-BFRS of 27 ppt m s^{-1} (Farmer and Cohen, 2007). That NO_x flux was estimated to be no more than 1/3 due to soil emissions with the balance likely HONO emissions or due to an unknown source. Soil NO_x emissions have been shown to exhibit an exponential relationship with temperature (van Dijk et al., 2002; Williams et al., 1992). The estimated soil term of 9 ppt m s^{-1}, diluted into an 800 m boundary layer it represents ~40 ppt/h. Over a 5 h transit time, these emissions could account for a large fraction of the source that maintains near constant NO_x and of the approximately 700 ppt increase in NO_y that we observe, if they follow the exponential temperature pattern.

The ratio of NO/NO_2 during mid-afternoon showed a weak correlation with temperature (slope=–0.0020°C^{-1}, R^2=0.063, and increasing by about +17% from 18–32°C)). This ratio is controlled by the photolysis of NO_2 and oxidation of NO by oxidants such as O_3, HO_2 and RO_2. A rapid steady-state is established during midday at locations

ACPD
7, 11091–11121, 2007

removed from large NO_x sources that can be represented as:

$$j_{NO_2}[NO_2]=k_{NO+O_3}[NO][O_3] + k_{NO+RO2}[NO][HO_2 + RO_2] \quad (5)$$

where j_{NO2} is the rate constant of the photolysis reaction $NO_2+h\nu \rightarrow NO+O$ (UCAR/NCAR/ACD), k_{NO+O3} the rate constant for the reaction of $NO+O_3 \rightarrow NO_2+O_2$ (Sander et al., 2006), and k_{NO+ROx} the average rate constant for the reaction of $NO+RO_2$ and $NO+HO_2 \rightarrow NO_2+RO$, OH which we approximate as the rate constant for reaction of HO_2 with NO. Rate constants are taken from Sander et al. (2006).

For days that we have simultaneous measurements of NO, NO_2 and O_3 we estimate the HO_2+RO_2 concentrations using Eq. (5). The afternoon averages were 200 ppt with a 100 ppt variance. However, the HO_2+RO_2 values derived from the NO/NO_2 ratio is quite noisy and affected substantially by uncertainty in the NO instrument's measurement of zero. Within the envelope of the noise and our estimates of the effects of the uncertainty in the NO instrument zero, we estimate the maximum trend in peroxy radicals that would be consistent with the data is +47% and the minimum is –25%. This is a weaker temperature-dependence than suggested by our interpretation of the HNO_3 and ΣPN data as implying increases in OH of a factor of 2–3. OH increases that are this large would normally be accompanied by HO_2+RO_2 increases of 40–200% assuming the peroxy radicals increase with OH concentration with a dependence between linear and as the square root. This implies that most of the increase in OH occurred upwind, perhaps in closer proximity to the isoprene emissions, or that a chemical process that alters the HO_2+RO_2 to OH ratio is active.

3.6 O_3

The strong correlation of O_3 with temperature shown in Fig. 4 is typical for a rural site. This slope of 2.2 ppb/°C is similar to that reported for other rural sites at a similar temperature range (3±1, ~3–5, respectively) (Olszyna et al., 1997; Sillman and Samson, 1995) and is slightly higher (~3 ppb/°C) if peak ozone rather than the early afternoon

average is used (as was used in the calculations, Sillman and Sampson, 1995). Inspection of the diurnal cycles of O_3, shown in Fig. 2, suggests that this relationship with temperature is due both to increases in production rates for single days but also to accumulation during multi-day events where carryover from the previous day is important.

4 Discussion

Our results bear some similarities to the results of Olszyna et al. (1997), who report that the ratio PAN/NO_y decreased with increasing temperature with a slope of –0.015°C^{-1}, that NO_z increased from 55 to 75% of NO_y, that NO_x/NO_y decreased from 45 to 25%, that PAN/NO_y decreased from 35 to 20%, that [HNO_3 + particulate nitrate] was unchanged, and that the "missing NO_y" increased from 0 to 20% over an ambient temperature range of 25°C to 30°C. We observe a slope for $\Sigma PNs/\Sigma NO_{yi}$ of –0.015°C^{-1}, identical to the PAN/NO_y slope reported by Olyszna et al. In contrast to Olszyna et al.'s observation, we see a much larger increase in HNO_3/NO_y and equating their "missing NO_y" with our ΣANs we observe a much smaller increase of $\Sigma ANs/NO_y$. Other reports of correlations of reactive nitrogen species with temperature include positive correlations of HNO_3 and negative correlations of PAN for three different seasons (summer, spring, and winter) (Bottenheim and Sirois, 1996), a negative correlation of PAN and temperatures for a yearlong dataset (Gaffney and Marley, 1993), and increases of PAN with temperature during summer (Schrimpf et al., 1998). In addition, several models discussing effects of climate change predict decreases in ΣPN concentrations (e.g., Steiner et al., 2006; Stevenson et al., 2005).

Since the model discussed in Sillman and Sampson (1995) is the most complete and comparable discussion in the literature of the relationship of temperature and reactive nitrogen partitioning in a rural environment, it is valuable to discuss in some more length the similarities and differences between their model and our measurements. They model rural sites in Michigan and Alabama for a summer day and describe changes in

midday OH, HO_2, O_3, HNO_3, ΣPNs and ΣANs, and NO_x concentrations vs. the daily maximum temperature. For these two sites, over the temperature range we consider in this paper (18–32°C), they show relative changes in ΣPNs of –50%, ΣANs of +50% to as much +150%, and little to no change in NO_x or HNO_3. Although our observations of ΣPNs and NO_x closely match those predictions, this is likely fortuitous because of the large differences between the predictions of HNO_3 and ΣANs and our observations.

In the Sillman and Sampson calculations most of the additional NO_x available from decreasing ΣPNs forms ΣANs, making ΣANs the dominant contribution to NO_z at higher temperatures. They attribute this large rise in ΣANs to increasing isoprene emissions producing isoprene nitrates. They used a yield of 10% for alkyl nitrate formation from reaction of NO with isoprene peroxy radicals, and a slow deposition velocity for isoprene nitrates. Comparison of our observations of ΣANs on the DC-8 to a global model show that parameters that are more consistent with the ΣAN measurements are a yield of 4% and a rapid deposition rate, one that is similar to that of HNO_3 (Horowitz et al., 2006). These adjustments to the model would also free up NO_x that would partially be converted to HNO_3 resulting in increased HNO_3 at higher temperatures.

Nevertheless, it is surprising that Sillman and Sampson (1995) predict nearly constant HNO_3 since they show predicted changes in OH (for the Michigan site) in which OH nearly doubles over the relevant temperature range. Since no significant increase in HNO_3 accompanies this OH increase, the formation rate of ANs, consuming the available NO_x, must increase much faster in the model – preesumably because isoprene is a more effective NO_x sink in the model than at our site. Also in contrast to our observations, other researchers have predicted that with increased isoprene, PNs (and ANs) will increase at the expense of HNO_3 (Lopez et al., 1989; Trainer et al., 1991). Further research is needed to understand if these differences between models and our observations reflect different situations or if they provide a generally useful diagnostic.

Increases in OH with high temperature were predicted by Sillman and Sampson (1995), who showed they would be due to increases in both O_3 and H_2O in the Eastern U.S. At the UC-BFRS, there is no increase in H_2O concentration with temperature;

ACPD
7, 11091–11121, 2007

O_3 increases by 65% from 18–32°C (Fig. 4) and if only considering the effect of the primary production rate of OH ($O_3 + h\nu \rightarrow 2OH$) this would account for 65% of the OH increase. A likely more important factor is the increase in upwind sources of isoprene and its oxidation products which are exponentially related to temperature, increasing by approximately a factor of 15 from 18 to 32°C (Dreyfus et al., 2002). CH_2O, which is calculated to be nearly equal in importance to O_3 as an HO_x source at the UC-BFRS, is a major product of isoprene oxidation, and a direct HO_x source. Also, there are now several direct observations of OH and indirect measures of the influence of OH showing that OH is increased above model predictions in environments rich in biogenic VOC (Farmer and Cohen, 2007; Kuhn et al., 2007).

5 Conclusions

We have presented measurements of the effects of ambient temperature (18–32°C) on the atmospheric mixing ratios of a nearly complete suite of speciated reactive nitrogen. We observe that there is a small decrease in NO_x/NO_y, a large increase in HNO_3/NO_2, a decrease in ΣPNs and an increase in ΣANs with increasing temperature. Analysis of the results show small changes in NO_x and $\Sigma NO_{y,i}$ indicating a near balance in temperature-dependant NO_x sources, NO_x oxidation rates, and permanent NO_z losses in relatively aged air. However, large changes in the ratios of the different oxides suggests a large temperature dependent increase in OH. This increase cannot be explained by temperature dependent increases in O_3 or H_2O. Increases in H_2CO are also likely too small, leading us to suggest that there are chemical processes associated with isoprene emissions (and thus indirectly with temperature) that are not accurately represented in current chemical mechanisms. This conjecture is consistent with the analysis of Thornton et al. (2002) and more recent laboratory and field data (Hasson et al., 2004; Kuhn et al., 2007; Ren et al., 2007[1]; Stickler et al., 2007).

[1]Ren, X., Olson, J. R., Crawford, J. H., Brune, W. H., Mao, J., Long, R. B., Chen, G., Avery, M. A., Sachse, G. W., Barrick, J. D., Diskin, G., Huey, L. G., Fried, A., Cohen, R. C., Heikes, B.,

There are few measurements of the effects of temperature on NO_y speciation where there were sufficient observations to track the nitrogen budget. The one prior measurement that was nearly as comprehensive as the one described here, was much closer to the source region, and thus there is little overlap of the NO_x/NO_y ratio (or approximate photochemical age) of the two data sets. Still, the results are similar in the region of overlap suggesting that our results might be representative of many locations and not special because of their location in the foothills of the Sierra Nevada downwind of Sacramento. Our results are quite different than prior model calculations. We observe a larger increase in the contribution of HNO_3 to NO_z and to NO_y with temperature and a smaller increase in alkyl nitrates than predicted by in Sillman and Sampson (1995). The latter of these is probably in part due to the high yield (10%) and low deposition velocity used in that model, whereas there is growing evidence suggesting that smaller yields and more rapid deposition velocities for isoprene nitrates are what is occurring in the atmosphere.

In light of these and other improvements in our understanding of atmospheric chemistry, it would be valuable to revisit the temperature dependence of precursors to ozone more systematically in current models to assess whether they are consistent with the observations of NO_{yi} and inferences about OH presented herein and to assess our current understanding of the likely effects of climate change on air quality.

Acknowledgements. We gratefully acknowledge support for the observations by the NASA Instrument Incubator Program under Contract #NAS1-99053 and support for the analysis by the U.S. Environmental Protection Agency through grant RD-83096401-0 to the University of California, Berkeley. "Although the research described in this article has been funded wholly or in part by the U.S. Environmental Protection Agency through grant RD-83096401-0 to the University of California, Berkeley, it has not been subjected to the Agency's required peer and policy review and therefore does not necessarily reflect the views of the Agency and no official endorsement should be inferred." We also thank the staff of UC-BFRS for their support and SPI for access to the research site.

Wennberg, P. O., Singh, H. B., Blake, D. R., and Shetter, R. E.: HO_x observations and model comparison during INTEX-A 2004, J. Geophys. Res., submitted, 2007.

References

Bauer, M. R., Hultman, N. E., Panek, J. A., and Goldstein, A. H.: Ozone deposition to a ponderosa pine plantation in the Sierra Nevada Mountains (CA): a comparison of two different climatic years, J. Geophys. Res.-A., 105, 22 123–22 136, 2000.

Bertram, T. H. and Cohen, R. C.: A Prototype Instrument for the Real Time Detection of Semi-Volatile Organic and Inorganic Nitrate Aerosol, Eos Trans. AGU, 84(46), Fall Meet. Suppl., Abstract A51F-0740, 2003.

Bottenheim, J. W. and Sirois, A.: Long-Term Daily Mean Mixing Ratios of O-3, Pan, Hno3, and Particle Nitrate At a Rural Location in Eastern Canada - Relationships and Implied Ozone Production Efficiency, J. Geophys. Res.-A., 101, 4189–4204, 1996.

Brown, S. S., Dibb, J. E., Stark, H., Aldener, M., Vozella, M., Whitlow, S., Williams, E. J., Lerner, B. M., Jakoubek, R., Middlebrook, A. M., DeGouw, J. A., Warneke, C., Goldan, P. D., Kuster, W. C., Angevine, W. M., Sueper, D. T., Quinn, P. K., Bates, T. S., Meagher, J. F., Fehsenfeld, F. C., and Ravishankara, A. R.: Nighttime removal of NOx in the summer marine boundary layer, J. Geophys. Res.-A., 31, L07108, doi:10.1029/2004GL019412, 2004.

Cardelino, C. A. and Chameides, W. L.: Natural Hydrocarbons, Urbanization, And Urban Ozone, J. Geophys. Res.-A., 95, 13 971–13 979, 1990.

Carroll, J. J. and Dixon, A. J.: Tracking the Sacramento pollutant plume over the western Sierra Nevada. Final Report to California Air Resources board under Interagency Agreement #94-334. 26 pages plus appendicies., http://www.arb.ca.gov/research/apr/past/atmospheric.htm, 1998.

Cleary, P. A., Wooldridge, P. J., Millet, D. B., McKay, M., Goldstein, A. H., and Cohen, R. C.: Observations of total peroxy nitrates and aldehydes: measurement interpretation and inference of OH radical concentrations, Atmos. Chem. Phys., 7, 1947–1960, 2007, http://www.atmos-chem-phys.net/7/1947/2007/.

Day, D. A.: Observations of NO_2, Total Peroxy Nitrates, Total Alkyl Nitrates, and HNO_3 in the Mid-Sierras and Sacramento Plume Using Thermal Dissociation – Laser Induced Fluorescence, Ph. D. thesis, 207 pp, University of California at Berkeley, Berkeley, Ca, 2003.

Day, D. A., Dillon, M. B., Wooldridge, P. J., Thornton, J. A., Rosen, R. S., Wood, E. C., and Cohen, R. C.: On Alkyl Nitrates, O_3, and the "Missing NO_y", J. Geophys. Res.-A., 108, 4501, doi:10.1029/2003JD003685, 2003.

Day, D. A., Wooldridge, P. J., Dillon, M. B., Thornton, J. A., and Cohen, R. C.: A thermal dissoci-

ation laser-induced fluorescence instrument for *in situ* detection of NO_2, peroxy nitrates, alkyl nitrates, and HNO_3, J. Geophys. Res.-A., 107, 4046, doi:10.1029/2001JD000779, 2002.
Dillon, M. B.: The Chemical Evolution of the Sacramento Urban Plume, Ph. D. thesis, 206 pp, University of California, Berkeley, 2002.
Dillon, M. B., Lamanna, M. S., Schade, G. W., Goldstein, A. H., and Cohen, R. C.: Chemical evolution of the Sacramento urban plume: Transport and oxidation, J. Geophys. Res.-A., 107, 4045, 10.1029/2001JD000969, 2002.
Dreyfus, G. B., Schade, G. W., and Goldstein, A. H.: Observational constraints on the contribution of isoprene oxidation to ozone production on the western slope of the Sierra Nevada, CA, J. Geophys. Res.-A., 107, 4365, doi:10.1029/2001JD001490, 2002.
Farmer, D. K. and Cohen, R. C.: Observations of HNO_3, ΣAN an ΣPN and NO_2 fluxes: Evidence for rapid HO_x chemistry within a pine forest canopy, Atmos. Chem. Phys. Discuss., 7, 7087–7136, 2007, http://www.atmos-chem-phys-discuss.net/7/7087/2007/.
Fountoukis, C., Sullivan, A., Weber, R., Vanreken, T., Fischer, M., Matias, E., Moya, M., Farmer, D. K., and Cohen, R. C.: Thermodynamic characterization of Mexico City Aerosol during MILAGRO 2006, Atmos. Chem. Phys. Discuss., 7, 9203–9233, 2007, http://www.atmos-chem-phys-discuss.net/7/9203/2007/.
Gaffney, J. S. and Marley, N. A.: Measurements of Peroxyacetyl Nitrate at a Remote site in the Southwestern United States: Tropopheric Implications, Environ. Sci. Technol., 27, 1905–1910, 1993.
Goldstein, A. H., Hultman, N. E., Fracheboud, J. M., Bauer, M. R., Panek, J. A., Xu, M., Qi, Y., Guenther, A. B., and Baugh, W.: Effects of climate variability on the carbon dioxide, water, and sensible heat fluxes above a ponderosa pine plantation in the Sierra Nevada (CA), Agric. Forest Meteorol., 101, 113–129, 2000.
Hasson, A. S., Tyndall, G. S., and Orlando, J. J.: A product yield study of the reaction of HO2 radicals with ethyl peroxy (C2H5O2), acetyl peroxy (CH3C(O)O-2), and acetonyl peroxy (CH3C(O)CH2O2) radicals, J. Phys. Chem. A, 108, 5979–5989, 2004.
Herman, D. J., Halverson, L. J., and Firestone, M. K.: Nitrogen dynamics in an annual grassland: oak canopy, climate, and microbial population effects, Ecol. Appl., 13, 593–604, 2003.
Hogrefe, C., Biswas, J., Lynn, B., Civerolo, K., Ku, J. Y., Rosenthal, J., Rosenzweig, C., Goldberg, R., and Kinney, P. L.: Simulating regional-scale ozone climatology over the eastern United States: model evaluation results, Atmos. Environ., 38, 2627–2638, 2004

Horowitz, L. W., Fiore, A. M., Milly, G. P., Cohen, R. C., Perring, A., Wooldridge, P. J., Hess, P. G., Emmons, L. K., and Lamarque, J.-F.: Observational constraints on the chemistry of isoprene over the Eastern U.S., J. Geophys. Res., 112, D12S08, doi:10.1029/2006JD007747, 2007.

Kleinman, L., Lee, Y. N., Springston, S. R., Nunnermacker, L., Zhou, X. L., Brown, R., Hallock, K., Klotz, P., Leahy, D., Lee, J. H., and Newman, L.: Ozone Formation At a Rural Site in the Southeastern United-States, J. Geophys. Res.-A., 99, 3469–3482, 1994.

Kuhn, U., Andreae, M. O., Ammann, C., Araújo, A. C., Brancaleoni, E., Ciccioli, P., Dindorf, T., Frattoni, M., Gatti, L. V., Ganzeveld, L., Kruijt, B., Lelieveld, J., Lloyd, J., Meixner, F. X., Nobre, A. D., Pöschl, U., Spirig, C., Stefani, P., Thielmann, A., Valentini, R., and Kesselmeier, J.: Isoprene and monoterpene fluxes from Central Amazonian rainforest inferred from tower-based and airborne measurements, and implications on the atmospheric chemistry and the local carbon budget, Atmos. Chem. Phys., 7, 2855–2879, 2007, http://www.atmos-chem-phys.net/7/2855/2007/.

Kurpius, M. R., McKay, M., and Goldstein, A. H.: Annual ozone deposition to a Sierra Nevada ponderosa pine plantation, Atmos. Environ., 36, 4503–4515, 2002.

Lamb, B., Guenther, A., Gay, D., and Westberg, H.: A National Inventory Of Biogenic Hydrocarbon Emissions, Atmos. Environ., 21, 1695–1705, 1987.

Lefer, B. L., Talbot, R. W., and Munger, J. W.: Nitric acid and ammonia at a rural northeastern U.S. site, J. Geophys. Res.-A., 104, 1645–1661, 1999.

Leung, L. R. and Gustafson, W. I.: Potential regional climate change and implications to US air quality, Geophys. Res. Lett., 32, L16711, doi:10.1029/2005GL022911, 2005.

Lopez, A., Barthomeuf, M. O., and Huertas, M. L.: Simulation of chemical processess occurring in an atmopheric boundary layer. Influence of light and biogenic hydrocarbons on the formation of oxidants., Atmos. Environ., 23, 1465–1478, 1989

Murazaki, K. and Hess, P.: How does climate change contribute to surface ozone change over the United States?, J. Geophys. Res.-A, 111, D05301, doi:10.1029/2005JD005873, 2006.

Murphy, J. G., Day, A., Cleary, P. A., Wooldridge, P. J., and Cohen, R. C.: Observations of the diurnal and seasonal trends in nitrogen oxides in the western Sierra Nevada, Atmos Chem. Phys., 6, 5321–5338, 2006a

Murphy, J. G., Day, D. A., Cleary, P. A., Wooldridge, P. J., Millet, D. B., Goldstein, A. H., and Cohen, R. C.: The weekend effect within and downwind of Sacramento: Part 1. Observations of ozone, nitrogen oxides, and VOC reactivity, Atmos. Chem. Phys. Discuss., 6, 11 427–

11 464, 2006b.
Murphy, J. G., Day, D. A., Cleary, P. A., Wooldridge, P. J., Millet, D. B., Goldstein, A. H., and Cohen, R. C.: The weekend effect within and downwind of Sacramento: Part 2. Observational evidence for chemical and dynamical contributions, Atmos. Chem. Phys. Discuss., 6, 11 971–12 019, 2006c.
Olszyna, K. J., Bailey, E. M., Simonaitis, R., and Meagher, J. F.: O3 And Noy Relationships At A Rural Site, Geophys. Res. Lett., 99, 14 557–14 563, 1994.
Olszyna, K. J., Luria, M., and Meagher, J. F.: The correlation of temperature and rural ozone levels in southeastern USA, Atmos. Environ., 31, 3011–3022, 1997.
Parrish, D. D., Norton, R. B., Bollinger, M. J., Liu, S. C., Murphy, P. C., Albritoon, D. L., Fehsenfeld, F. C., and Heubert, B. J.: Measurements of HNO3 and NO3 pariculates at a rural site in the Colorado mountains, J. Geophys. Res.-A., 91, 5379–5393, 1986.
Rosen, R. S., Wood, E., Wooldridge, P. J., Thornton, J. A., D.A., D., Kuster, B., Williams, E. J., Jobson, B. T., and Cohen, R. C.: Observations of total alkyl nitrates during TEXAQS-2000Observations of total alkyl nitrates during Texas Air Quality Study 2000: Implications for O-3 and alkyl nitrate photochemistry, J. Geophys. Res.-A., 107, D07303, doi:10.1029/2003JD004227, 2004.
Rubin, J. I., Kean, A. J., Harley, R. A., Millet, D. B., and Goldstein, A. H.: Temperature dependence of volatile organic compound evaporative emissions from motor vehicles, J. Geophys. Res.-A., 111, D03305, doi:10.1029/2005JD006458, 2006.
Sander, ..., and ... (2006), Chemical kinetics and photochemical data for use in atmospheric studies, Evaluation number 15; NASA Panel for Data Evaluation, edited, National Aeronautics and Space Administration; Jet Propulsion Laboratory California Institute of Technology, Pasadena, California.
Schrimpf, W., Linaerts, K., Muller, K. P., Koppmann, R., and Rudolph, J.: Peroxyacetyl nitrate (PAN) measurements during the POPCORN campaign, J. Atmos. Chem., 31, 139–159, 1998.
Seaman, N. L., Stauffer, D. R., and Lariogibbs, A. M.: A Multiscale 4-Dimensional Data Assimilation System Applied in the San-Joaquin Valley During Sarmap .1. Modeling Design and Basic Performance-Characteristics, J. Appl. Meteorol., 34, 1739–1761, 1995.
Sillman, S. and Samson, F. J.: Impact of Temperature On Oxidant Photochemistry in Urban, Polluted Rural and Remote Environments, J. Appl. Meteorol., 100, 11 497–11 508, 1995.
Steiner, A. L., Tonse, S., Cohen, R. C., Goldstein, A. H., and Harley, R. A.: Influence of future

climate and emissions on regional air quality in California, J. Geophys. Res.-A., 111, D18303, doi:10.1029/2005JD006935, 2006.
Stevenson, D., Doherty, R., Sanderson, M., Johnson, C., Collins, B., and Derwent, D.: Impacts of climate change and variability on tropospheric ozone and its precursors, Faraday Discussions, 130, 41–57, 2005.
Stickler, A., Fischer, H., Bozem, H., Gurk, C., Schiller, C., Martinez-Harder, M., Kubistin, D., Harder, H., Williams, J., Eerdekens, G., Yassaa, N., Ganzeveld, L., Sander, R., and Lelieveld, J.: Chemistry, transport and dry deposition of trace gases in the boundary layer over the tropical Atlantic Ocean and the Guyanas during the GABRIEL field campaign, Atmos Chem. Phys. Discus., 7, 4781–4855, 2007.
Stump, F. D., Knapp, K. T., Ray, W. D., Snow, R., and Burton, C.: The Composition Of Motor-Vehicle Organic Emissions Under Elevated-Temperature Summer Driving Conditions (75-Degrees-F To 105-Degrees-F), Journal Of The Air & Waste Management Association, 42, 152–158, 1992.
Thornton, J. A., Wooldridge, P. J., and Cohen, R. C.: Atmospheric NO_2: In situ laser-induced fluorescence detection at parts per trillion mixing ratios, Anal. Chem., 72, 528–539, 2000.
Thornton, J. A., Wooldridge, P. J., Cohen, R. C., Martinez, M., Harder, H., Brune, W. H., Williams, E. J., Fehsenfeld, F. C., Hall, S. R., Shetter, R. E., Wert, B. P., and Fried, A.: Observations of ozone production rates as a function of NO_2 abundances and HO_x production rates in the Nashville urban plume, J. Geophys. Res., 107, 4146, doi:10.1029/2001JD000932, 2002.
Trainer, M., Buhr, M. P., Curran, C. M., Fehsenfeld, F. C., Hsie, E. Y., Liu, S. C., Norton, R. B., Parrish, D. D., Williams, E. J., Gandrud, B. W., Ridley, B. A., Shetter, J. D., Allwine, E. J., and Westberg, H. H.: Observations and Modeling of the Reactive Nitrogen Photochemistry At a Rural Site, J. Geophys. Res.-A., 96, 3045–3063, 1991.
UCAR/NCAR/ACD: Tropospheric Ultraviolet and Visible (TUV) Radiation Model, http://cprm.acd.ucar.edu/Models/TUV/, 2006.
van Dijk, S. M., Gut, A., Kirkman, G. A., Meixner, F. X., Andreae, M. O., and Gomes, B. M.: Biogenic NO emissions from forest and pasture soils: Relating laboratory studies to field measurements, J. Geophys. Res.-A., 107, 8058, doi:10.1029/2001JD000358, 2002.
Welstand, J. S., Haskew, H. H., Gunst, R. F., and Bevilacqua, O. M.: Evaluation of the effects of air conditioning operation and associated environmental conditions on vehicle. emissions and fuel economy, Tech. Pap. Ser., 2003-01-2247, 2003

Wiedinmyer, C., Greenberg, J., Guenther, A., Hopkins, B., Baker, K., Geron, C., Palmer, P. I., Long, B. P., Turner, J. R., Petron, G., Harley, P., Pierce, T. E., Lamb, B., Westberg, H., Baugh, W., Koerber, M., and Janssen, M.: Ozarks Isoprene Experiment (OZIE): Measurements and modeling of the "isoprene volcano", J. Geophys. Res.-A., 110, D18307, doi:10.1029/2005JD005800, 2005.

Williams, E. J., Guenther, A., and Fehsenfeld, F. C.: An Inventory of Nitric-Oxide Emissions from Soils in the United-States, J. Geophys. Res.-A., 97, 7511–7519, 1992.

Williams, E. J., Roberts, J. M., Baumann, K., Bertman, S. B., Buhr, S., Norton, R. B., and Fehsenfeld, F. C.: Variations in NO_y composition at Idaho Hill, Colorado, J. Geophys. Res.-A., 102, 6297–6314, 1997.

Zhang, Q., Carroll, J. J., Dixon, A. J., and Anastasio, C.: Aircraft measurements of nitrogen and phosphorus in and around the Lake Tahoe Basin: Implications for possible sources of atmospheric pollutants to Lake Tahoe, Environ. Sci. Technol., 36, 4981–4989, 2002.

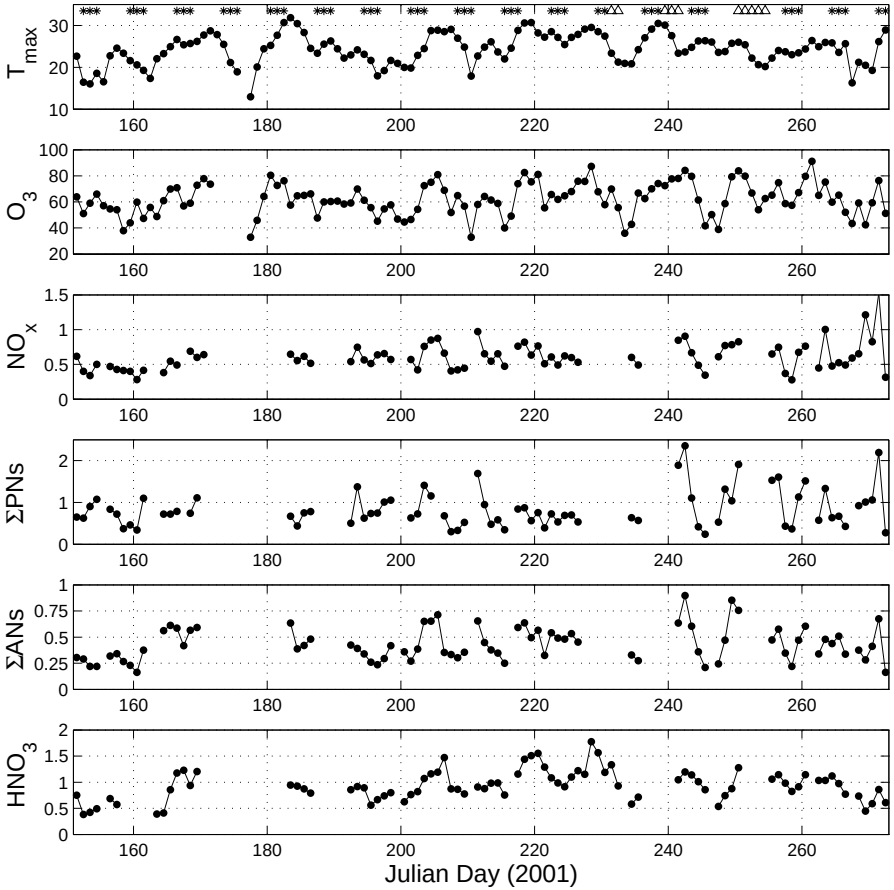

Fig. 1. Daily temperature maxima (T_{max}) and daily averages (medians) of O_3, ΣNO_{yi}, NO_x, ΣPNs, ΣANs, and HNO_3 for hours 12–16 for 1 June–30 September 2001. Symbols on top panel represent: non-weekday (asterisks) and days where trace gas species were excluded from the analysis due to impact of forest fires (triangles).

ACPD
7, 11091–11121, 2007

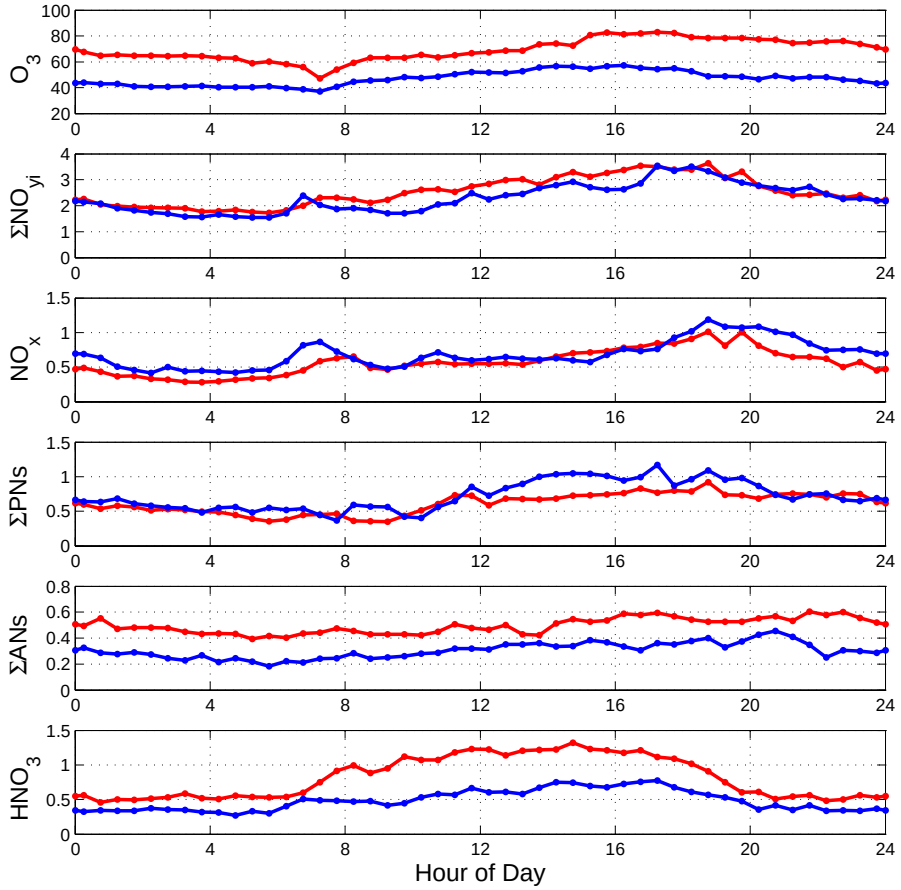

Fig. 2. Diurnal cycles of O_3, ΣNO_{yi}, NO_x, ΣPNs, ΣANs, and HNO_3 shown for half-hour intervals of the 17th and 83rd percentile of the measurements as ordered by the associated daily temperature maximum (T_{max}); T_{max} 17th percentile = 20.8°C (blue), T_{max} 83rd percentile 28.4°C (red).

ACPD
7, 11091–11121, 2007

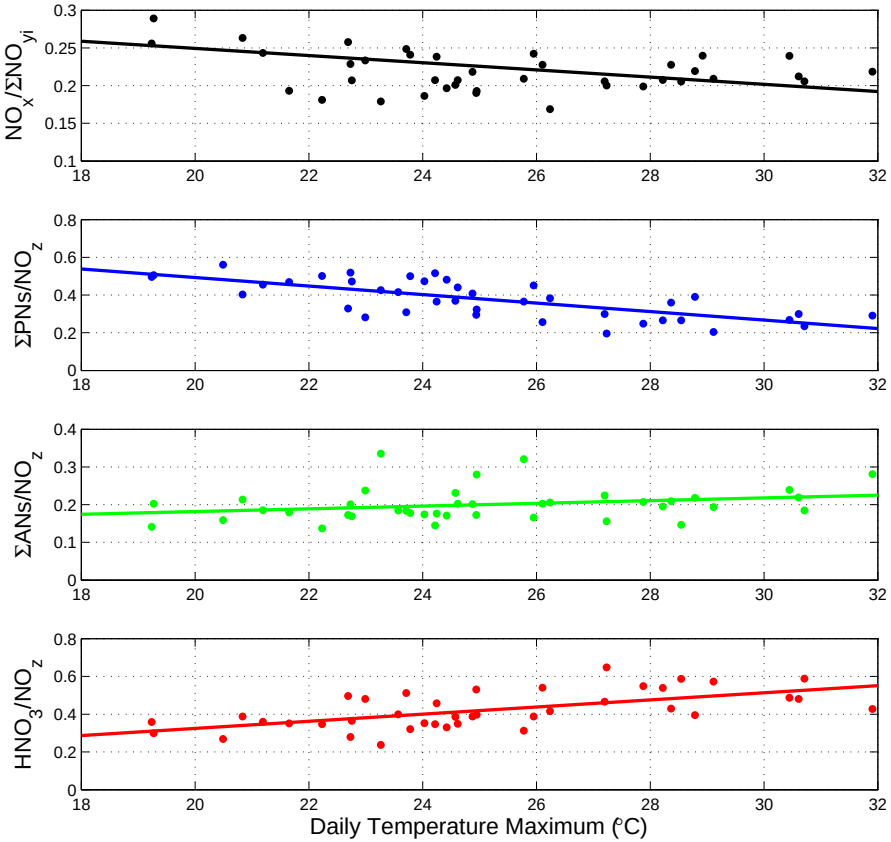

Fig. 3. $NO_x/\Sigma NO_{yi}$ $\Sigma PNs/NO_z$, $\Sigma ANs/NO_z$, and HNO_3/NO_z averaged (median) for single daily values during hours 12-16 vs. daily temperature maximum. Least-squares fit lines shown from top to bottom have parameters: slopes = –0.0048, –0.023, 0.0036, 0.019 and R^2 values = 0.14, 0.52, 0.069, and 0.37.

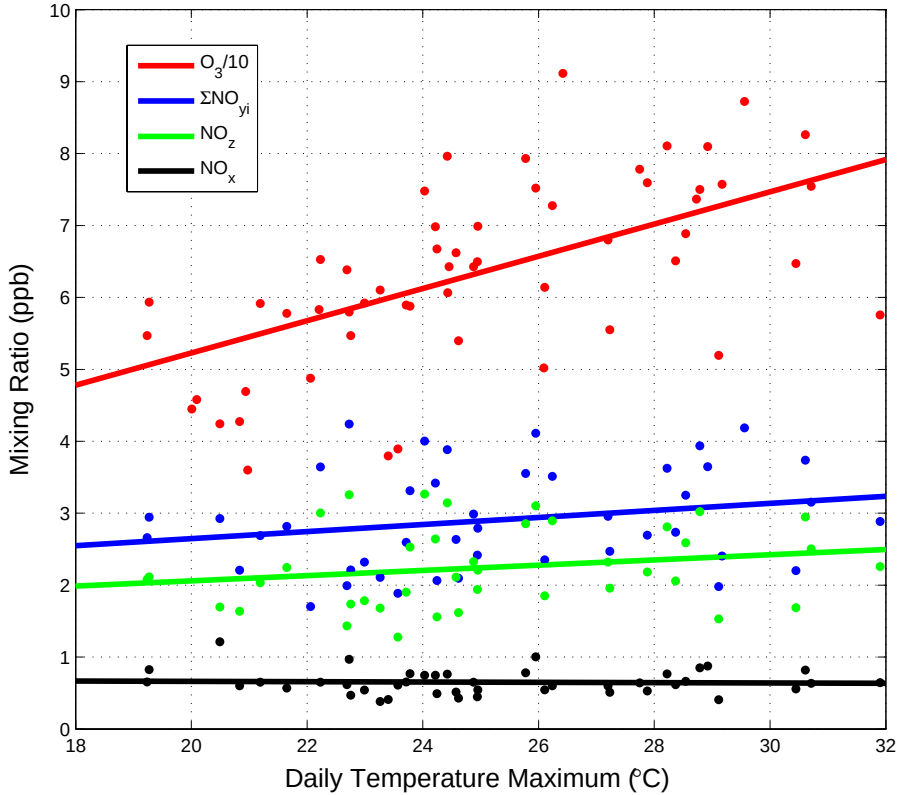

Fig. 4. O_3, ΣNO_{yi}, NO_z, and NO_x averaged (median) for single daily values during hours 12–16 vs. daily temperature maximum. Best fit lines shown have parameters (from top to bottom): slopes = 2.24, 0.049, 0.036, –0.0007 and R^2 values = 0.43, 0.052, 0.043, 0.002.

ACPD
7, 11091–11121, 2007

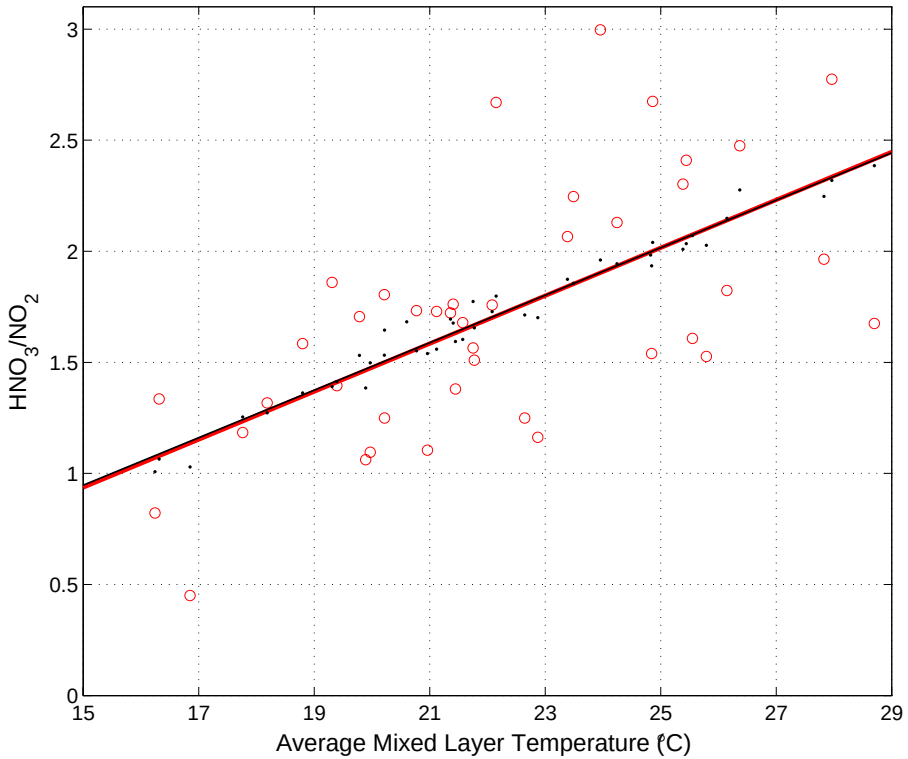

Fig. 5. HNO_3/NO_2 averaged (median) for single daily values during hours 12–16 vs. average mixed layer temperature. Observations (red circles), modeled values (black points), and the coincident best fit lines are shown.

ACPD
7, 11091–11121, 2007